Case Study for Thermo Mechanical Performance of an Integrated Optic Device via Equation-Based Modelling

Seval DÖNERTAŞ[1,2*] (iD), Mutlu GÖKKAVAS[2] (iD), Ekmel ÖZBAY[2,3] (iD), Elif ÖZ ORHAN[1,4] (iD)

[1]Gazi University, Department of Advanced Technologies, 06560, Ankara, Turkey
[2]Bilkent University, Nanotechnology Research Center (NANOTAM), 06800, Ankara, Turkey
[3]Bilkent University, Department of Electrical and Electronics Engineering, 06800, Ankara, Turkey
[4]Gazi University, Department of Physics, 06560, Ankara, Turkey

Keywords	Abstract
Integrated Optical Device *Multiphysics* *Finite Element Analysis*	An integrated optical device was modeled in the simulation environment via Comsol software. Model implementation, meshing analysis, the definition of material parameters, analyze and module type was introduced, respectively. At the end of this paper; it was understood that the connection of the bodies with different thermal expansion coefficients causes thermal stress accumulation and deformation. The acquired results reveal that fiber-based components can be analyzed with the contribution of the simulation interface. The literature researches were examined in detail and it was found that no study discusses the modeling of the full structure of the fiber optic integrated optic device. So; this study is crucial because it explains how to model an integrated optic device via simulations and leads the researchers about how to make complex meshing analysis in the presence of thin epoxy layers.

1. INTRODUCTION

Integrated optics is an area combining fiber-optic and waveguiding technologies. Before signal transmission by light beams, electrical currents or radio waves were the preferred way to convey signals over long distances (Richter,1989). With the development of fiber optics communication systems, advances in microfabrication technologies, integrated optical technology has emerged as an enabling technology. Low power consumption, smaller size, lower loss, and better reliability ensure that integrated optics is more preferable over competing technologies where available. Lightwave communications, control of microwave components, sensor systems, and data processing are a few application areas of integrated optics technology (John, 1997).

In general, electro-optic phase modulators are known as the simplest integrated optical devices which have applications in defense, navigation and space technologies. In these devices, the joint between an optical chip and input/output fiber is produced by the application of ultraviolet (UV) transparent epoxy. In this paper, we will study a Y-junction integrated optical device (Yang et al., 2014). Explicitly, it splits the incoming light signal into two arms at the end of the waveguide. The proposed integrated optical device is a lithium niobate ($LiNbO_3$) based component. Actually, in telecommunication applications, $LiNbO_3$ has high electro-optic coefficients in the near-infrared region of the spectrum, so this material is preferred in the fabrication process of the electro optic modulators (Wooten et al., 2000). Besides this; high Curie

temperature (1100°C-1180°C) of LiNbO$_3$ material enables it sufficient to produce low-loss waveguides via metal diffusion (Wooten et al., 2000). Especially; because LiNbO$_3$ has more than %80 optical transparency at the 1.55 µm telecommunication wavelength, it is a favorable material in optoelectronic applications. After the alignment of the waveguide arms of the LiNbO$_3$ based optical device and fiber optic pigtail carriers, input and output fibers are glued to both of the device arms. The final product is called a "fiber-coupled integrated optical device" (Tripathi et al., 2007).

Literature surveys about the mechanical behavior at the interface between the fiber-coupled device and optical fiber under thermal variations are investigated. In one research, the deformation was analyzed at the connection region between optical chip and fiber under temperature changes, so thermomechanical simulations at the coupling structure were progressed via finite element analysis (FEA) (Yao et al., 2018).

The reliability of the fiber optic current sensors was studied by conducting thermal tests (Lenner et al., 2017). Also; in this research, the effect of materials with different thermal expansion coefficients was considered to specify the failure modes.

According to another investigation, it is explained that stress is evaluated among basic factors of the mechanical breakdown between chip/epoxy junction (Suchoski and Boivin, 1992). Moreover, the failure of this coupling interface is extremely critical when considered other breakdown mechanisms for integrated optical chips.

Although several studies have been conducted about the mechanical strength of the integrated optical devices, it is clear that detailed investigations related to the theoretical analysis are relatively limited in the publications. So; this paper aims to examine the mechanical durability of the fiber-coupled devices via thermomechanical simulations by using three dimensional (3D) finite element analysis (FEA) method. In this context; the detailed expressions about simulation software, the construction of three-dimensional structural geometry, meshing types, material parameters, boundary conditions, analysis type, and module type were given, respectively. At the end of this study; it is obvious that the motivation related to the thermal simulation of fiber optic devices enhances.

2. MATERIAL AND METHOD

In this study, simulations were performed with COMSOL 5.5 Multiphysics commercial software by using FEA-based equations. COMSOL is a simulation program compatible with modeling experimental applications in a software environment. To solve complex physical problems comprehensively and scientifically, the "COMSOL multiphysics interface" was introduced to this software. Several different modules are combined in the "COMSOL multiphysics interface" such as acoustics, electromagnetics, chemical reactions, mechanics, fluid flow, and heat transfer (Anonymous, 2020a). Since the subject of this study is the investigation of thermomechanical performance, heat transfer, and solid mechanics software modules were utilized for the analysis.

The integrated fiberoptic device-under-study consists of three basic parts: fiber pigtail carriers, optical fibers, optical chip, and waveguide regions as shown in Figure 1. In addition to this, the electrodes which are shown in the figure are employed to create an electro-optic response while driving the device.

2.1. 3D Modelling

At the beginning of the simulation, the 3D geometrical structure of the integrated optical device was modeled with the actual dimensions. The main body of the configuration is an optical chip and its parameters are as follows: optical chip length along y-direction: 24 mm, width along x-direction: 2.6 mm, thickness along z-direction: 1 mm. The detailed structure is illustrated in Figure 2.

As shown in Figure 2; input/output fiber pigtail carriers incorporate two separate components: upper and bottom lower parts. Besides this, the optical fibers are sandwiched between upper and bottom pigtail carriers by sticking with a UV curable epoxy. Since there is a thickness difference between the optical chip

and pigtail carriers, two symmetric covers were attached to the input and output device ends. All of the device components are connected with UV curable epoxy.
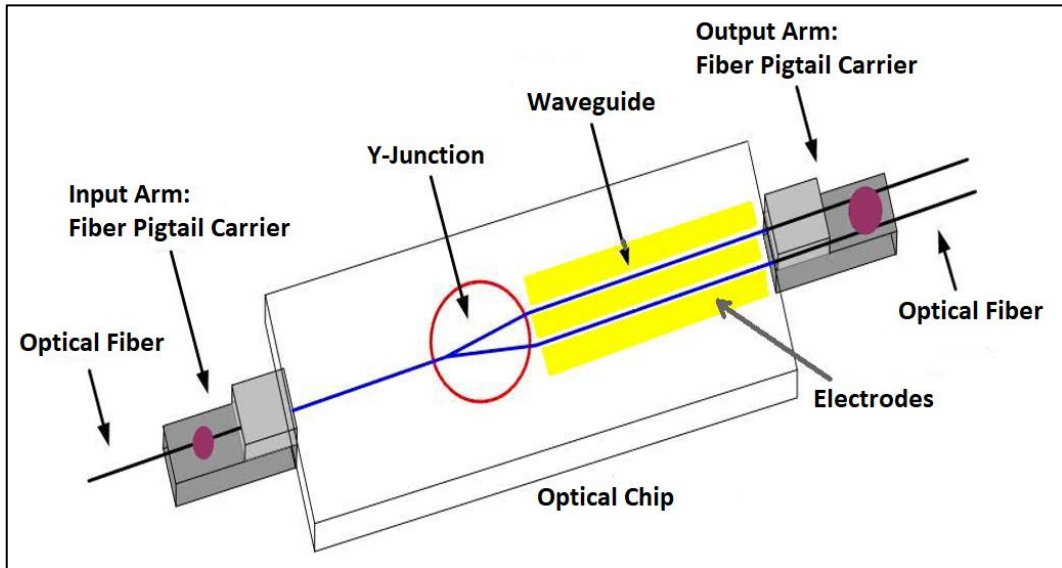

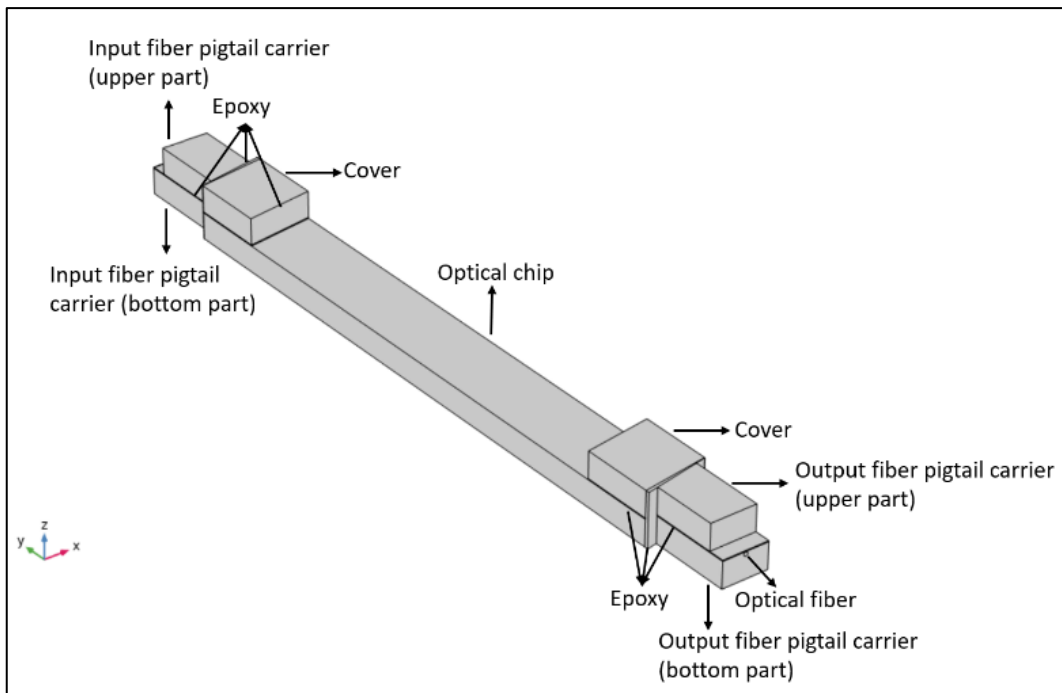*Figure 1. Schematic Configuration of the Integrated Optical Device*

Figure 2. 3D Model of the Integrated Optical Device Structure

2.2. Meshing Analysis

Meshing analysis has a crucial effect on any simulation study. In COMSOL; there are two different meshing types: i) user-controlled, ii) physics-controlled. While physics controlled option enables automatic mesh construction, user-controlled mesh allows manual element size adjustments (Alvarado et al., 2013). The modeled integrated optical device includes a large number of parts with varying size and aspect ratio parameters. During the study, it was observed that physics-controlled mesh is not well suited for such structures due to the incompatibilities at the junction points. Although the default meshing sequence type for the simulation interface is a physics-controlled mesh type, different meshing element types can not be used with physics-controlled mesh and the usage of only one default element type is forced. As it is

mentioned before, the model structure in this paper includes many parts with different dimensions. Because of this reason, all of these parts can not be meshed with only one element type, otherwise, the discrepancies at the junction regions arise due to the aspect ratio incompatibilities and connection faults of the mesh nodes. On the other hand; user-controlled mesh type allows the operator to build and edit the meshing sequence manually. Also for this mesh type, mesh elements can be resized as required. Therefore, a user-controlled meshing type was chosen instead of physics controlled mesh. In Figure 3; the mesh construction of the whole geometry is shown.
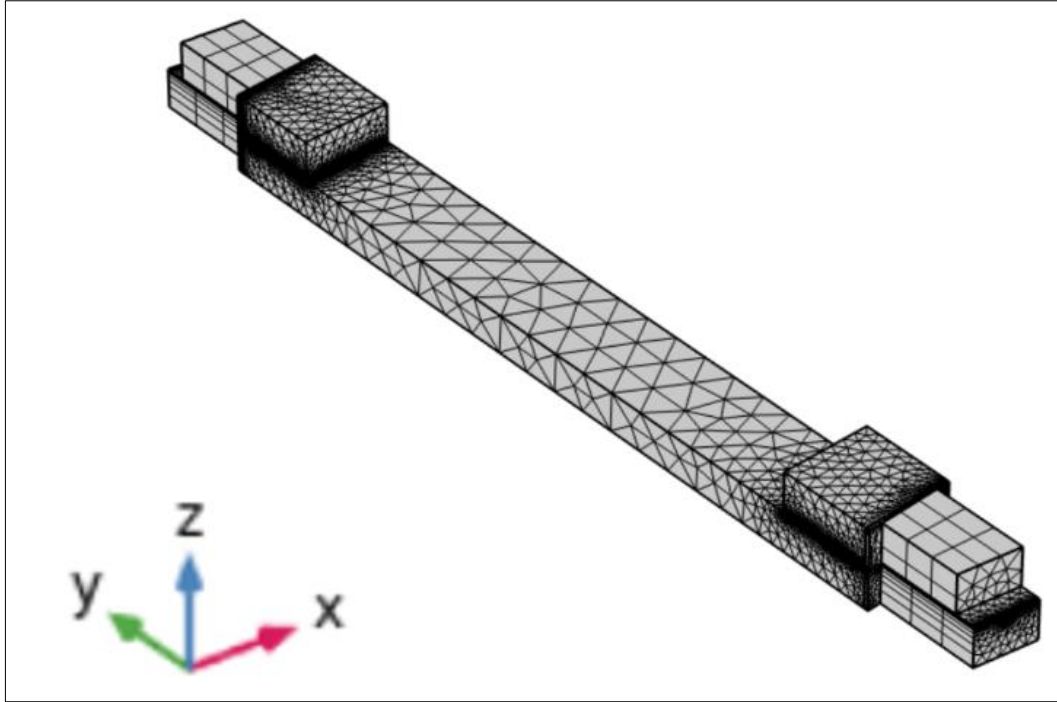

Figure 3. *Meshed Model*

It can be seen in Figure 3 that the densities, types, and sizes of the domains differ from each other. To make a comprehensive evaluation, the mesh parameters are listed in Table 1.

Table 1. *Mesh Statistics for the Defined Geometry*

Domain	Optical Chip	Fiber Pigtail Carrier	Cover	Epoxy	Optical Fiber
Mesh Type	Tetrahedral	Triangular/Swept	Tetrahedral	Tetrahedral	Triangular/Swept
Mesh Size	Extremely Fine	Extra Fine	Extremely Fine	Finer	Extra Fine
Mesh Element Number	35268	3621	28949	14678	198

Three different element types (tetrahedral, triangular, and swept) were preferred in the simulation. Especially, the variation of stress distribution on the epoxy domains at the fiber/optical chip joint requires a good discretization of these regions. While the thickness of the epoxy parts is approximately 40 µm, the rest of the parts are on the order of millimeters. Since the high aspect ratio between epoxy domains and the other parts makes the mesh solution challenges, the correct choice of mesh element type has a drastic influence on the stress calculation results. Below, we list a detailed description of the different mesh types:

The swept mesh type is known as a geometrical discretization technique in "Comsol Multiphysics" and is generally used for thin geometries and structures. It starts at a source boundary region and sweeps along a defined destination boundary (Anonymous, 2020b). Since fiber pigtail carriers are proven commercial products, these areas were not our major region of interest during our study. Application of the swept mesh type can be more convenient for such regions. Therefore, upper and bottom pigtail carrier parts, optical fibers, and the epoxy domains between upper and bottom parts were meshed with triangular and swept mesh types.

The tetrahedral element type is the basic and simplest one among others for most "Comsol Multiphysics" applications. Any domain can mesh with tetrahedral independent from the geometry (Anonymous, 2020c). The triangular element type can be used in some special circumstances. Since mesh algorithms generally need more input for this element type, it can not be used for every geometry. The primary cause of using triangular elements is that they can decrease mesh density (Anonymous, 2020c). There is a basic difference between tetrahedral and triangular mesh types. While triangular have high aspect ratios, the aspect ratio is limited to unity for tetrahedral mesh elements. In those cases where the analysis results are not crucial, it is favorable to use a triangular element type. In the context of this paper; since the fiber pigtail carriers, the epoxies between upper and bottom fiber pigtail carriers, and optical fibers results are not analyzed, swept and triangular mesh types were preferred for these components. The second reason for using these mesh types is that there is a high aspect ratio between optical fiber, epoxies, and the carriers. On the other hand, the tetrahedral mesh type is chosen for the rest of the domains due to the low aspect ratio.

2.3. Material Parameters

The material parameters defined for the integrated optical device are listed in Table 2. The materials of the constitutive parts are $LiNbO_3$ (Filatov et al., 2016), UV curable (Anonymous, 2021a) and SiO_2 (Anonymous, 2021b).

Table 2. Physical Parameters of the Materials

Domain	Material	ρ (kg/m^3)	E (GPa)	η	k (W/(m.K)	α(x10^{-6}) (1/K)
Optical Chip/Cover/ Pigtail Carriers	$LiNbO_3$	4690	170	0.25	5.6	2.0 and 16.7
Epoxy	UV Curable	1290	1.03	0.48	0.15	65
Optical Fiber	SiO_2	2170	66.3	0.15	1.30	0.55

A brief description of the parameters (ρ, density; E, Young's Modulus; η, Poisson's ratio; k, thermal conductivity, and α, coefficient of thermal expansion) listed in Table 2 is included below: These quantities are used in the heat transfer and solid mechanics calculations to solve the related equations. While Young's Modulus and Poisson's ratio terms are necessary parameters for the structural stability calculations, thermal conductivity, density, and coefficient of thermal expansion parameters belong to heat transfer calculations. According to the partial differential equation included in the heat transfer interface (Anonymous, 2020d), ρ and α are the parameters that are used in the related theoretical equation. Especially; the thermal expansion coefficient is one of the parameters which is incorporated in the derivation of thermoelastic damping. In Comsol Multiphysics; the expression of the heat flux by conduction is demonstrated with q and given as $k * \nabla T$. In this equation; k is the thermal conductivity that accounts for the calculation of heat flux expression. Besides the heat transfer theory, the rest of the terms which are included in Table 2 are required to solve equations for solid mechanics interface. Young's Modulus and Poisson's Ratio are the basic characteristic parameters that are utilized to solve the structural deformation of the materials. In Comsol Multiphysics; these material parameters have importance to make structural analyses of the simulated model. Many of the stress calculations in Comsol Multiphysics are based on elastic strain equations

(Anonymous, 2020e). In general; strain means the deformation of a material because of the stress effect. Elastic strain tensor is derived after eliminating inelastic deformations from the displacements. For the linear analysis; elastic strain is given with the equation $\varepsilon_e = \varepsilon - \varepsilon_{inel}$ (Anonymous, 2020e). Here; ε_e, ε and ε_{inel} are elastic, total, and inelastic strain tensor statements, respectively. There is a correlation between the Poisson's ratio and strain. Poisson's ratio; is the ratio of transverse contraction strain to longitudinal extension strain. Because the materials react to deform under thermal stress, particularly the Poisson's ratio is a crucial material parameter to calculate deformations in the structure. Just as strain, stress is another parameter to define geometrical changing of material. In a simulation environment; since Young's Modulus is essential to indicate how the material is bent or changes its shape under thermal or structural stresses, this property is a basic parameter for the related solid mechanics equations.

Besides, since $LiNbO_3$ is a uniaxial material, the properties along the x and y-axis are equal to each other, but the parameters along the z-axis are different. Thus, two different thermal expansion coefficients are defined for $LiNbO_3$ material.

2.4. Boundary Conditions

Thermal and boundary conditions were assigned to solve the equations in the heat transfer and solid mechanics environments. First of all; the temperature boundary condition was applied to the bottom surface of the optical chip and both of the fiber pigtail carriers, holding these surfaces at a temperature T(t). In the solid mechanics section, a rigid motion suppression boundary condition is added to all of the domain parts. This constraint adds a minimum number of constraints to suppress rigid body motions (Anonymous, 2020e). Since all of the parts are bonded to each other by gluing, rigid motion suppression was applied to all of the domains. The motivation for the choice of this option can be explained as follows: in one simulation study (Anonymous, 2020f), rigid motion suppression was added to one of the two domains which were glued to each other, aiming the prevention of rigid body motion in at least one body. So, the reason why this boundary condition is preferred in our simulation study is that all of the domains are attached with some kind of epoxy. Moreover; in the referenced study, enabling structural stability for thermal expansion problems is proposed. Another boundary condition for solid mechanics is related to the anisotropic properties of $LiNbO_3$ which is a piezoelectric material. Since this kind of material is an anisotropic material, its physical properties are orientation-dependent (Zhang, 2012). In the fabrication process, x-cut y-propagation $LiNbO_3$ material was used. For the x-cut y-propagation material, while the waveguide is extended along the -y axis, the electrical field is applied along the z-axis to obtain maximum modulation coefficient, and also x-axis is normal to the crystal surface (Liu et al., 2019). In Figure 4; the x-cut $LiNbO_3$ substrated structure is demonstrated.
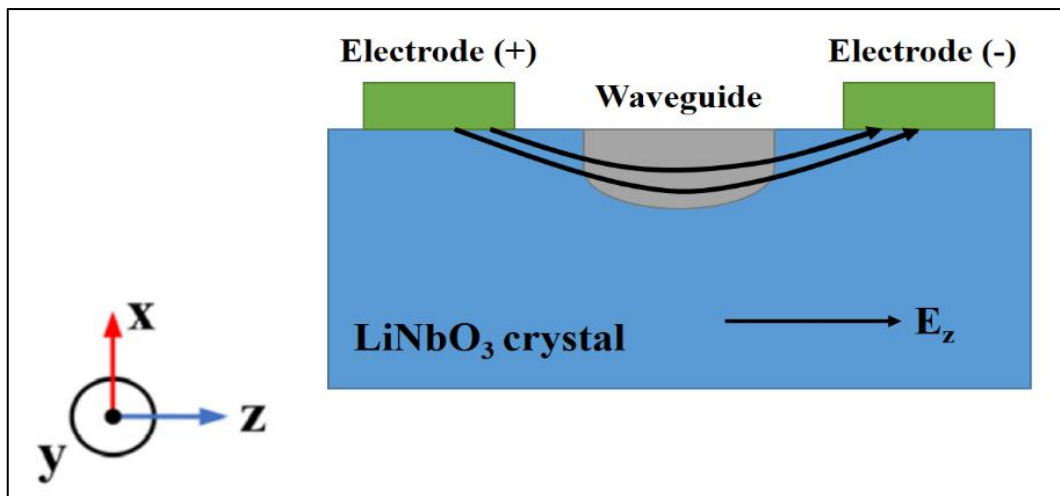

Figure 4. x-cut LiNbO₃ Crystal Orientation

A transformation vector set was specified to correspond to the crystal coordinate system with the material coordinate system, called a "base vector coordinate system". This vector system allows creating an orthogonal coordinate system in Comsol as shown in Figure 5. In the left configuration; it is seen that the

x, y, z-axis were transformed as corresponding with their self colors. In the right notation; it is seen that the base vector coordinate system is expressed with the matrix form.
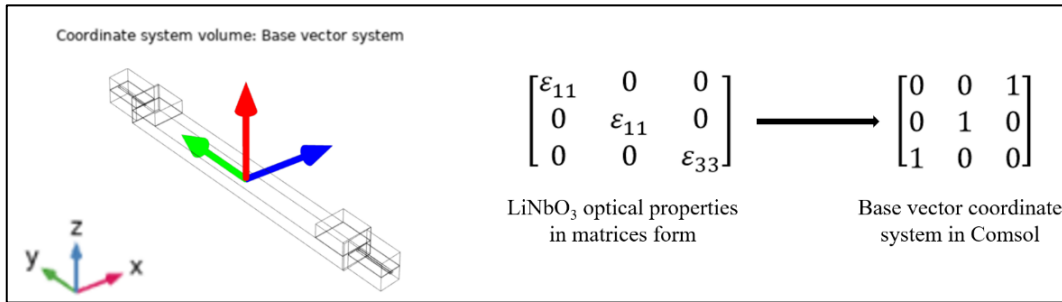

Figure 5. *Base Vector Coordinate System and Matrix Form for the Crystal Orientation*

2.5. Analyzation Type and Conditions

Thermomechanical simulations were carried out via time-dependent analysis. The time-dependent analysis is preferred when variables change in the time domain. For example; the heat transfer process can be used to calculate the temperature variations over time. Moreover; in solid mechanics applications, determination of the time-dependent deformation changes in the basic application area of this analysis method. In this paper; a temperature profile between -40°C and +85°C with 1°C/min. temperature rate was applied as shown in Figure 6. While at the heating process, the temperature is constant between 95.min-125.min time intervals, at the cooling process, it is constant between 255.min-285.min time intervals.
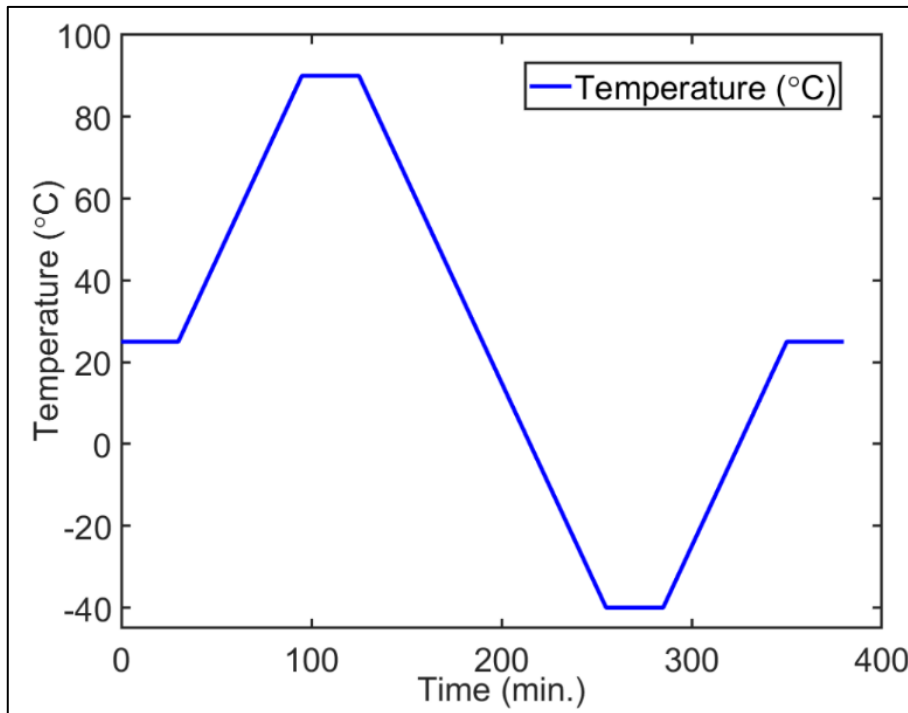

Figure 6. *Time-Dependent Temperature Profile*

2.6. Equation-Based Solutions for the Heat Transfer and Solid Mechanics Modules

The problems were solved using equation-based modeling. Basically; COMSOL operates according to the finite element model (FEM). FEM is a numerical technique to generate solutions that are defined by partial differential equations (PDE) (Nikishkov, 2004). The required model specifications can be created based on mathematical equations and they can be directly incorporated into the software's graphical interface (Anonymous, 2020g). These properties provide all of the models to be controlled. With equation-based modeling, expressions and mathematical terms can be introduced to the system. Some equation types such

as partial differential equations (PDE), algebraic equations, ordinary differential equations (ODE) can be solved using this modeling type. Especially, it is stated that a set of linear algebraic equations should be preferred for linear problems (Nikishkov, 2004).

In this study; temperature-dependent stress analysis was performed via equation-based modeling by associating heat transfer and solid mechanics interfaces. The solved equations are indicated in Equations 1 and 2.

$$\rho Cp(\frac{\partial T}{\partial t})_+ \rho C_p u.\nabla T + \nabla . (-k\nabla T) = Q + Q_{ted} \tag{1}$$

$$\sigma = \sigma_0 + C: (\epsilon - \epsilon_0 - \alpha\theta) \tag{2}$$

Equation 1 represents the heat transfer energy equation where the parameters (T, temperature; ρ, density; C_p, specific heat capacity at constant pressure; u, the velocity vector of translational motion; k, thermal conductivity; Q, volumetric heat generation; Q_{ted}, thermoelastic damping) are defined. In this equation; the conservation of energy is explained in terms of temperature. Equation 2 is related to Hooke's law and explains the stress-strain relation of the material (Barbagallo et al., 2015). In the Equation 2; all given parameters (σ, final stress tensor; σ_0, initial stress tensor; C, elasticity tensor; ϵ, total strain tensor; ϵ_0, initial strain tensor; α, volumetric thermal expansion coefficient; θ, the relationship between local temperature and strain reference temperature) are related to the mechanical properties of the materials. Moreover, Equation 2 was calculated to sense the stress-strain which is affected by thermal causes (Barbagallo et al., 2015). So; in this study, both solid mechanics and heat transfer equations are combined to solve equation-based simulations.

2.7. Evaluation of Temperature, Stress, and Deformation Fields

In this section; the following analyses were evaluated: i) temperature and ii) stress/deformation fields on the whole structure, iii) time-dependent Von-Mises stress distribution on the epoxy domain between optical chip/fiber pigtail carrier.

In Figure 7; the temperature field of an integrated optical component is shown. This figure describes the thermal distribution at 85°C over the whole system and obtained by solving the heat transfer module via time-dependent analysis. The thermal distribution of the epoxy domain between the optical chip/fiber pigtail carrier interface changes at most a few temperatures.

Besides the thermal performance, the stress and deformation field of the integrated optical device were investigated as depicted in Figure 8(a-b).

Apart from Figure 2, in Figure 8(a-b); the upper and bottom parts of the fiber pigtail carrier are at the same dimensions. It was seen during simulations that solving time was considerably longer when these pieces were at different dimensions, resulting in convergence problems due to the complex mesh construction. It is known that stress variations on the fiber pigtail carriers are ignored during analyses. So; while evaluating stress/deformation fields, both of the parts of the pigtails were modeled as equal sizes to save solution time, and actual geometric sizes were disregarded. To calculate stress variation along the x, y, and z-axis separately, the total stress change called Von-Mises stress was considered in the evaluation of the results as shown in Figure 8(a). As can be seen from the figure, the stress level is varying over the epoxy region between the optical chip/fiber pigtail carrier interface. This difference originates basically due to the use of the materials with different thermal expansion coefficients. Moreover, there is a bit more stress accumulation at the corner of the cover rather than the rest of the regions. From the literature researches, the stress at these regions may arise most likely because of the geometrical singularity (Petrone et al., 2015). We can say that although there are not enough investigations related to mechanical simulations of the fiber optic devices, we have utilized published papers concerning the thermo-mechanical performance of other model structures to take as a reference. Besides this; deformation on the same epoxy region was investigated via total displacement. According to Figure 8(b); while maximum deformation with nearly 5 µm originates in the area between optical chip and carrier, the rest of the structure senses weak deformation close to zero.

When the literature survey is examined (Yao et al., 2018), this displacement value is in the reasonable micrometers range.
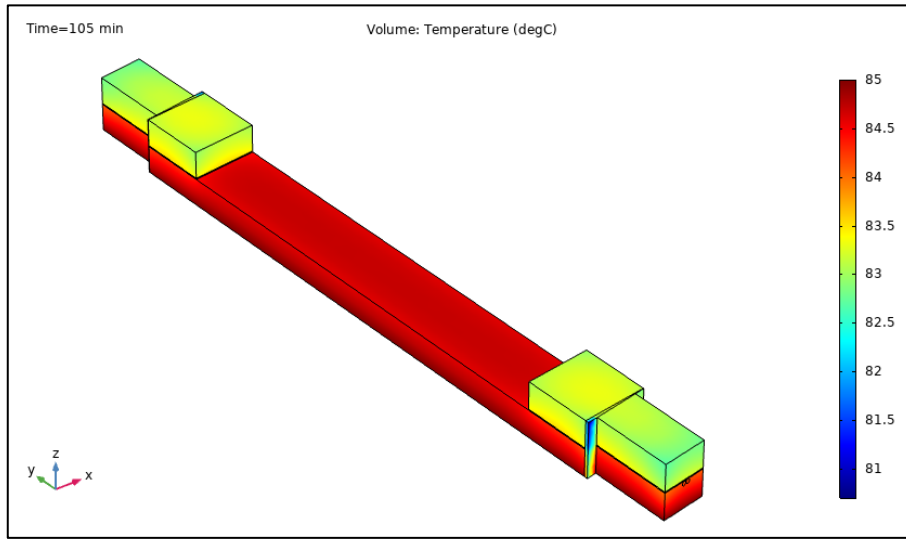

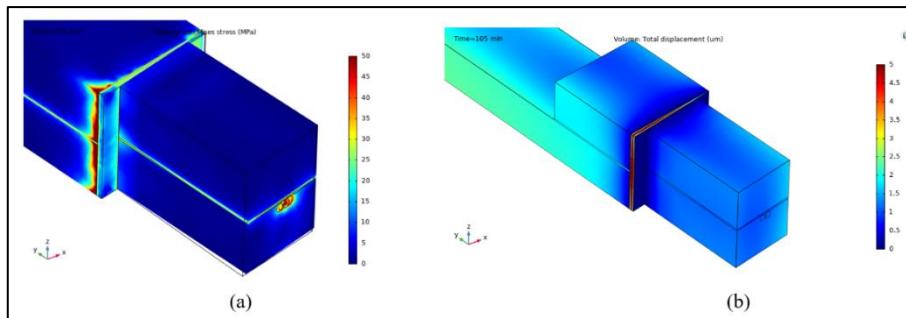**Figure 7.** *Temperature Field of the Integrated Optical Device at 85°C*

Figure 8. *Stress and Deformation Field of the Integrated Optical Device,*
(a) Stress Field, (b) Deformation Field

A typical device structure produced in the laboratory environment and the components of the integrated optical device are shown in Figure 9(a), while the corresponding model structure in the simulation environment is given in Figure 9(b). To analyze the Von-Mises stress distribution on the epoxy between the chip/carrier interface, the region marked as epoxy 1 region was taken into consideration.
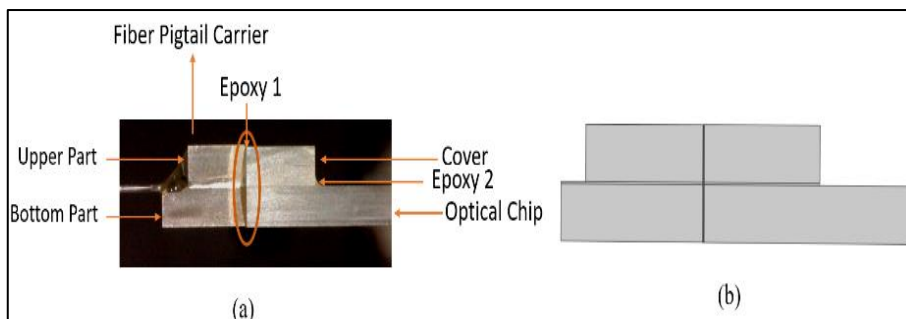

Figure 9. *Components of the Integrated Optical Device,*
(a) In the Experimental Environment, (b) In the Simulation Environment

The Von-Mises stress distribution versus time (temperature) result for the aforementioned temperature-time profile is shown in Figure 10(a). From the analyses, it was observed that Von-Mises stress increases as temperature increased. This figure shows the stress analysis between 60. min-150. min at around 85°C.

Increasement and decreasement trends of the stress parameter resemble the time-dependent temperature profile. As the temperature rises, stress ascends and also at the constant temperature between 95. min – 125. min, stress level also becomes stable. Similarly; when the temperature decreases further 120 min., the stress level descends below 100 MPa. In Figure 10(b); the analysis was carried out at constant time interval of 400 min for the temperature profile. In this case; the stress level increases gradually up to 200 MPa. It can be deduced that; when the time duration lengthens out, the stress level also increases from nearly 160 MPa to 220 MPa as shown in Figure 10(a-b).
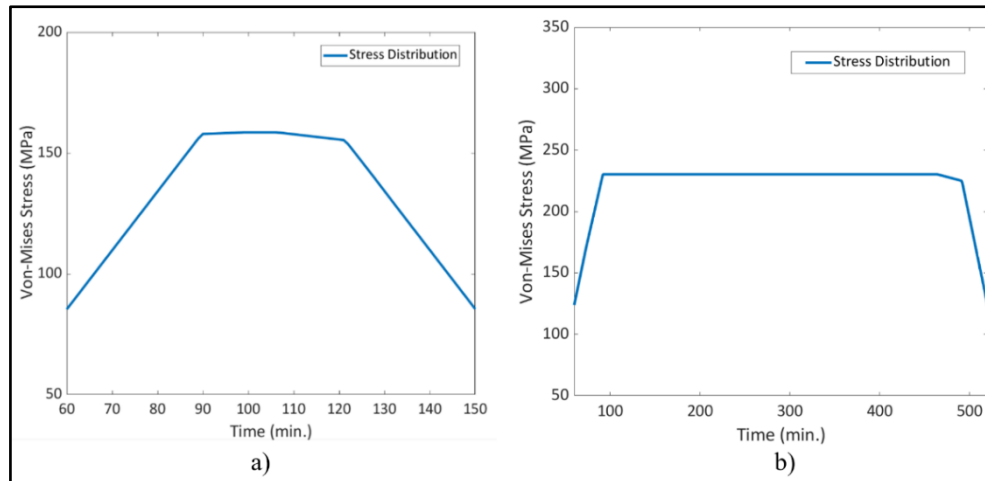

Figure 10. *Stress Fields on the Epoxy Between the Optical Chip and Fiber Pigtail Carrier,*
*(**a**) the Constant Time Interval is 30 min., (**b**) the Constant Time Interval is 400 min*

3. CONCLUSIONS

In this study; a method for thermomechanical stress analysis for an integrated optical device was proposed. The main improvement of this study is that simulation methods of the integrated optical device structures were introduced and the instructions were given in detail. The absence of such a study in the literature encouraged and motivated us to write this paper. According to the analyses; firstly, it was understood that thermal performance analyses of the fiber optic components can be carried out via equation-based simulation tools. In addition to this, the material properties such as anisotropicity of $LiNbO_3$ can be defined as a boundary condition. Since there is not much literature research related to thermal analysis of the integrated optical devices, this paper leads some guidelines in further researches and it showed that rather than stationary analysis, time-dependent solutions could be examined for this kind of structure.

In the future, simulation studies will be supported with experimental results. The results will be evaluated according to the changing of device geometry structures. These studies are currently in progression.

CONFLICT OF INTEREST

No conflict of interest was declared by the authors.

REFERENCES

Alvarado, R., Barlett, M., Beski, R., Isaza, S., & Li, C. (2013). Analysis of the thermo-mechanical reliability of an SMT attachment. (E-project-042513-011426) Project, Worcester Polytechnic Institute.

Barbagallo, C., Malgioglio, L. G., Petrone, G., & Cammarata, G. (2015). Thermo-mechanical analysis of a multi-chip power module. Conference on Thermal Energy Systems: Production, Storage, Utilization and the Environment.

Filatov, V. Y., Kukaev, S. A., Shalymov, V. E., & Venediktov, Y. V. (2016). Multiphysical simulations of passive ring cavities. Proceedings of SPIE, Optical Sensing and Detection IV, 9899, 98992X. doi:10.1117/12.2230223

John, F. (1997). Integrated optics. Industrial Applications of Lasers. Science Direct. Second Edition.

Lenner, M., Yang, L., Frank, A., & Bohnert, K. (2017). Long-term reliability of fiber-optic sensor components in harsh industrial environments. Advanced Photonics Congress. doi:10.1364/SENSORS.2017.SeW1E.3

Liu, J., Zhang, C., Zheng, Y., Song, J., Gao, F., & Yang, D. (2019). Suppression of nonlinear residual intensity modulation in the multifunction integrated optic circuit for fiber-optic gyroscopes. *Journal of Lightwave Technology*, *38*(6), 1572-1579. doi:10.1109/JLT.2020.2968478

Nikishkov, G. P. (2004). Introduction to the finite element method. [Lecture Notes] University of Aizu.

Petrone, G., Barbagallo, C., & Scionti, M. (2015). Thermo-mechanical analysis and fatigue life prediction for an electronic surface-mount device (SMD). Proceedings of COMSOL Conference.

Richter, P. (1989). Integrated optics: technology, devices and applications. *Periodica Polytechnica Chemical Engineering*, *34*(1-3), 205-212.

Suchoski, P.G., & Boivin, G.R. (1992). Reliability and accelerated aging of $LiNbO_3$ integrated optic fiber gyro circuits. Fiber Optic and Laser Sensors X, 1795, 38-47. doi:10.1117/12.141273

Tripathi, U.S., Dixit, N., Kaul, A. N., & Gupta, A.K. (2007). Multifunction integrated optic chip for FOG. Proceedings of the National Conference on Advances in Sensors for Aerospace Applications, Hyderabad.

Wooten, E.L., Kissa, M.K., Yi-Yan, A., Murphy, J.E., Lafaw, A.D., Hallemeier, F.P., Maack, D., Attanasio, V.D., Fritz, J.D., McBrien, J.G., & Bossi, E. D. (2000). A review of lithium niobate modulators for fiber-optic communications systems. *IEEE Journal of Selected Topics In Quantum Electronics*, *6*(1), 69-82. doi:10.1109/2944.826874

Yang, J., Yuan, Y., Zhou, A., Cai, J., Li, C., Yan, D., Huang, S., Peng, F., Wu, B., Zhang, Y., Liu, Z., & Yuan, L. (2014). Full evaluation of polarization characteristics of the multifunctional integrated optic chip with high accuracy. *Journal of Lightwave Technology*, *32*(22), 3641-3650. doi:10.1109/JLT.2014.2342753

Yao, J., Li, K., Li, B., Wang, C., Kan, C., She, X., & Shu, X. (2018). Study of wavelength temperature stability of multifunctional integrated optical chips applied on fiber-optic gyroscopes. *Journal of Lightwave Technology*, *36*(23), 5528-5535. doi:10.1109/JLT.2018.2875795

Zhang, G. (2012). Orientation of piezoelectric crystals and acoustic wave propagation. Proceedings of Comsol Conference.

Anonymous (2020a). (Accessed: 20/11/2020) www.comsol.com/blogs/what-is-comsol-multiphysics/

Anonymous (2020b). (Accessed: 21/11/2020) www.comsol.com/blogs/meshing-sweep-your-meshes-with-ease/

Anonymous (2020c). (Accessed: 22/11/2020) www.comsol.com/blogs/meshing-your-geometry-various-element-types/

Anonymous (2020d). User's Guide Heat Transfer Module. (Accessed: 23/11/2020) doc.comsol.com/5.4/doc/com.comsol.help.heat/HeatTransferModuleUsersGuide.pdf

Anonymous (2020e). User's Guide Structural Mechanics Module. (Accessed: 24/11/2020) doc.comsol.com/5.4/doc/com.comsol.help.sme/StructuralMechanicsModuleUsersGuide.pdf

Anonymous (2020f). (Accessed: 25/11/2020) www.comsol.com/blogs/how-to-provide-structural-stability-in-thermal-expansion-simulations/

Anonymous (2020g). (Accessed: 26/11/2020) https://www.comsol.com/blogs/3-examples-of-equation-based-modeling-in-comsol-multiphysics/

Anonymous (2021a). (Accessed: 13/01/2021) www.norlandprod.com/adhesives/NOA%2061.html

Anonymous (2021b). (Accessed: 14/012021) Comsol Material Library.